Nuclear Science and Techniques (2024) 35:133
https://doi.org/10.1007/s41365-024-01498-y

Determining beam transverse absolute position by triangulation of multi-electrode signal phase differences

Xing Yang[1,2] · Hong-Shuang Wang[1,2] · Yi-Mei Zhou[3] · Yong-Bin Leng[4]

Received: 13 November 2023 / Revised: 3 January 2024 / Accepted: 30 January 2024 / Published online: 23 July 2024

Abstract
Accurate measurement of the transverse position of a beam is crucial in particle accelerators because it plays a key role in determining the beam parameters. Existing methods for beam-position measurement rely on the detection of image currents induced on electrodes or narrow-band wake field induced by a beam passing through a cavity-type structure. However, these methods have limitations. The indirect measurement of multiple parameters is computationally complex, requiring external calibration to determine the system parameters in advance. Furthermore, the utilization of the beam signal information is incomplete. Hence, this study proposes a novel method for measuring the absolute electron beam transverse position. By utilizing the geometric relationship between the center position of the measured electron beam and multiple detection electrodes and by analyzing the differences in the arrival times of the beam signals detected by these electrodes, the absolute transverse position of the electron beam crossing the electrode plane can be calculated. This method features absolute position measurement, a position sensitivity coefficient independent of vacuum chamber apertures, and no requirement for a symmetrical detector electrode layout. The feasibility of this method is validated through numerical simulations and beam experiments.

Keywords Electron beam bunch-by bunch diagnostics · Bunch position measurement · Triangulation method · Bunch phase · Bunch-by-bunch · Transverse position · Pickup signal

1 Introduction

Transverse bunch position is an essential parameter that determines the characteristics of a bunched particle beam in an accelerator. Optimizing the operational performance of accelerator devices requires the precise measurement of the transverse position and fine-tuned control of the orbits at source points. This is crucial to enhance the operational efficiency of synchrotron radiation sources [1, 2]. The accurate measurement of the transverse position and precise control of the orbits at collision points are essential for optimizing the luminosity of colliders. The transverse position is influenced by factors such as closed orbit, Betatron oscillation, and orbit noise, making it significant in accelerator physics research. The beam measurement system determined the transverse position based on Eq. (1).

$$x(t) = x_0 + x_\beta + x_\epsilon(t) + x_c(t) + x_n(t), \tag{1}$$

where x_0 represents the static closed orbit, $x_\beta(t)$represents the displacement owing to Betatron oscillation, $x_\epsilon(t)$ represents the displacement caused by momentum dispersion, $x_c(t)$ represents the distortion caused by external factors such as magnet structure, and $x_n(t)$ represents the measurement system noise. Therefore, various types of information, including the closed orbit, beta function, dispersion function, transverse

This work was supported by the National Key R &D Program of China (No. 2022YFA1602201).

✉ Yong-Bin Leng
lengyb@ustc.edu.cn

[1] Shanghai Institute of Applied Physics, Chinese Academy of Sciences, Shanghai 201800, China

[2] University of Chinese Academy of Sciences, Beijing 100049, China

[3] Shanghai Advanced Research Institute, Chinese Academy of Sciences, Shanghai 201204, China

[4] University of Science and Technology of China, Hefei 230026, China

tune, transverse damping time, and transverse wake field, can be obtained by analyzing the transverse position data.

Currently, mainstream approaches for measuring the transverse bunch position can be categorized into two types based on the measurement targets. One method relies on the image current induced in detection electrodes, and the other is based on a narrowband wake field signal induced when a beam passes through a cavity structure. The waveforms of typical image current signals are described by Eq. (2) [3].

$$I_{\mathrm{b}}(t) = \frac{eN}{\sqrt{2\pi}\sigma_{\tau}} \exp\left(-\frac{\left(t-t_0\right)^2}{2\sigma_{\tau}^2}\right) \tag{2}$$

The signals contain information such as bunch charge (eN), bunch length (σ_{τ}), bunch arrival time (t_0), and signal amplitude ($I_{\mathrm{b}}(t)$). The transverse position of the beam bunch can be calculated by utilizing the amplitude of the image current signals induced on different electrodes under specific assumptions or approximations (e.g., the beam length remains constant, and the signal amplitude extraction method is independent of the signal arrival time), and the most commonly applied calculation method is the difference-over-sum algorithm. The detectors used in this method include button electrodes commonly used in electron storage rings [4–6], strip electrodes commonly used in electron linear accelerators [7–10], and shoe-box electrodes commonly used in hadron accelerators [11, 12]. Conversely, cavity beam position detectors typically consist of a reference cavity (typically a fundamental mode cavity) and position cavity (higher-order mode cavity). The signal waveforms of the two cavities are described by Eq. (3) [13].

$$\begin{aligned} V_0(t) &= A_0 q J_0\left(\frac{\chi_{01}\rho}{r}\right) e^{-\frac{t}{\tau_{010}}} \sin\left(\omega_{010}t+\varphi_0\right) \\ V_1(t) &= A_1 q J_1\left(\frac{\chi_{11}\rho}{r}\right) e^{-\frac{t}{\tau_{110}}} \sin\left(\omega_{110}t+\varphi_1\right) \end{aligned} \tag{3}$$

The reference cavity signal encompasses information such as beam bunch charge, beam bunch length, and beam bunch arrival time. The position cavity signal includes data beyond these parameters, such as the transverse position. By simultaneously considering the signal amplitudes of both cavities, the transverse position can be determined by normalizing the reference cavity signal using the position cavity signal. This method is commonly used in free-electron laser facilities owing to its high measurement resolution and long signal duration in the time domain [14–17].

Regardless of whether the method used to detect the image current or wake field, the obtained signals contained multiple physical quantities. Thus, completely decoupling them is impossible. Moreover, the assumed conditions, such as a constant bunch charge and length, should be satisfied. Otherwise, effects such as beam intensity and bunch length dependencies may arise. Furthermore, the position sensitivity factor in position-mapping relationships necessitates individual experimental measurements for the detection of the image current [18–20]. The information contained in the bunch signals, including phase information, was not utilized fully. Only the amplitude information was used in these methods. In addition, the phase of the reference cavity signal was independent of the transverse bunch position, and the phase of the position cavity provided information on only the transverse bunch deflection angle and had no measurable dependence on the transverse position offset.

An analysis of the operating principle of the image current method showed that the signal phase (signal arrival time) detected by the measurement system completely depended on the bunch arrival time, transverse position of the bunch, and transmission delay of the measurement system. The phase difference between different electrodes was determined by the beam bunch transverse position and measurement system delay between different channels. Therefore, we can identify a method that can accurately and promptly measure the phases of multi-electrode beam signals. The beam arrival time and system transmission delay can be analyzed based on a multi-electrode signal. By subtracting these from the original measurement phase, a signal-phase measurement quantity solely related to the transverse position of the beam cluster can be obtained. Subsequently, the transverse bunch position can be determined with absolute precision.

Since 2012, the Shanghai Synchrotron Radiation Facility (SSRF) beam instrumentation group has developed a three-dimensional position diagnostic method for electron storage rings, based on broadband random sampling technology. This method uses button electrodes as sources to couple signals, high-speed digital oscilloscopes as data acquisition devices, and offline software packages to analyze the massive amount of data collected by oscilloscopes. This method precisely measures the charge, transverse bunch position [21], longitudinal bunch phase [22, 23], synchrotron tune [24], and bunch purity [25]. Furthermore, an open-source software package called HOTCAP that can simultaneously performs three-dimensional position and charge measurements has been developed, and this package is applicable to any high-energy electron storage ring [26, 27]. The upgrade and transformation of the SSRF, including beam station technology and some accelerator subsystems, have greatly helped users [28, 29]. The beam position measurement system meets the upgraded requirements, but the optimization directions need to be explored further. Precise measurement of these parameters makes obtaining the transverse beam position through a phase possible. A comparison of the results of the traditional and new methods is crucial. The principle of using the arrival time difference to determine the position of the signal source has been

applied in numerous fields, such as PET systems [30, 31], scintillator fibers with PMTs at each end [32], and the time difference of arrival (TDOA) [33, 34]. However, measuring the beam position using this method is relatively new.

The document is organized as follows. A comprehensive exposition of the fundamental principles underlying the new method is provided in Sect. 2. Moreover, the following aspects are also discussed: the intricate mapping between the signal phase of the button electrodes and transverse bunch position, methodology for determining the transverse bunch position through the signal phase (arrival time), correlation between the phase measurement error and position measurement error, and calibration method of the measurement system. In Sect. 3, the results of numerical simulations conducted to analyze the new method are presented. The simulations included sensitivity analysis of the measurement systems, resolution evaluation, and injection process simulation. In Sect. 4, the results of confirmatory beam experiments, which include the observation of the injection process and assessment of the transverse instability of multiple bunches, are presented. The practicality and potential of these new methods are discussed in Sect. 5. Finally, conclusions are presented in Sect. 6.

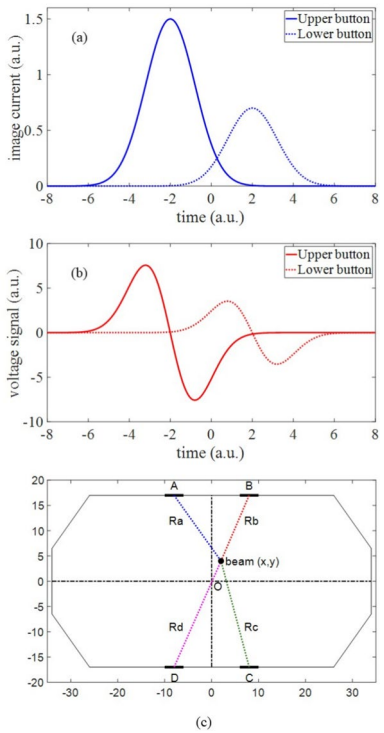

Fig. 2 **a** Image current waveform induced on the upper and lower pickup electrodes. **b** Voltage signal extracted from the upper and lower pickup electrodes. **c** SSRF storage ring octagonal vacuum chamber and four button electrode layout

2 Measurement Principle

To illustrate the measurement of the transverse position using the signal phase, a simplified example, wherein two electrode probes are used in a high-energy electron storage ring, is considered. The process of generating image currents in the bunch by passing it through a pair of detection electrodes is shown in Fig. 1.

The imaged current waveforms of the upper and lower electrodes are shown in Fig. 2a. The signal-voltage waveforms transmitted through the coaxial cable are shown in Fig. 2b.

When the bunch is close to the upper electrode, the image current signal amplitude on the upper electrode increases, resulting in a phase advance (blue and red solid lines in Figs. 2a and 2b). Conversely, as the bunch moves further away from the lower electrode, the image current

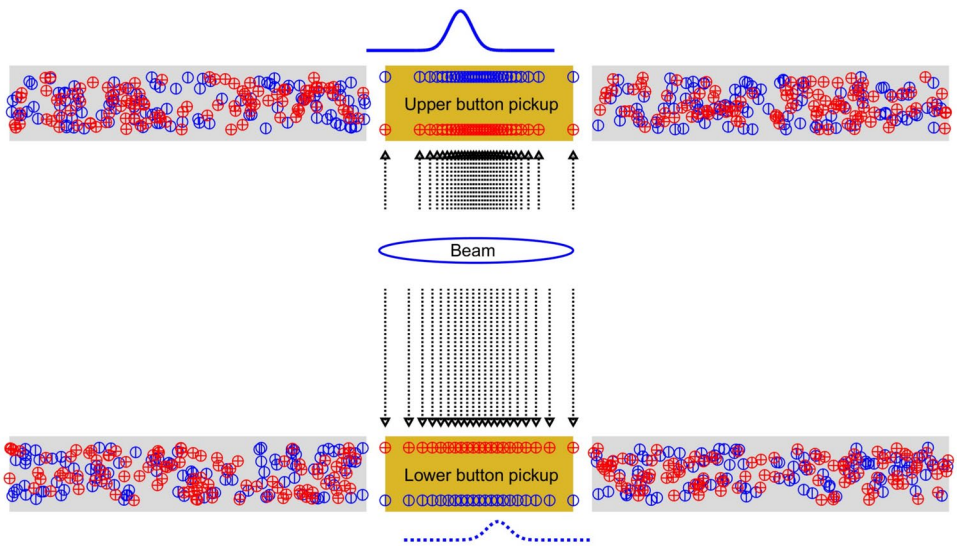

Fig. 1 (Color online) Schematic diagram of the image current induced by a relativistic electron bunch on a pickup electrode

Table 1 The caption of the table goes here

Height (mm)	34
Inner width (mm)	68
Electrode center to the *Y* central axis (mm)	8
Electrode center to the *X* central axis (mm)	17
Radius of electrodes (mm)	5

signal amplitude decreases, and the phase lags (blue and red dashed lines in Fig. 2a and 2b). The phase difference between the two-electrode signals was determined from the time delay between the propagation of the beam electric fields to the respective electrodes. The speed of electric field propagation is equivalent to the speed of light in vacuum, which is denoted by c. The distance between the beam bunch and electrodes can be obtained by multiplying the time difference by c.

Four electrodes were used in the beam position measurement system. The octagonal vacuum chamber and button electrode configurations in the SSRF storage ring are shown in Fig. 2c.

The specific parameters of the SSRF storage ring BPM chamber are shown in Table 1. A coordinate system was established on the plane on which the electrodes were placed in the vacuum chamber. The geometric centers of the four electrodes are denoted as O. The horizontal direction is the X-axis, and the vertical direction is the Y-axis. The distance from the electrode centers to the Y-axis is d, and the distance from the electrode centers to the X-axis is h.

When an electron bunch passes through the probe plane with position (x, y), the transverse distances R_a, R_b, R_c, and R_d between the bunch and four electrodes can be described by Eq. (4).

$$\begin{aligned} R_a &= \sqrt{(d+x)^2 + (h-y)^2} \\ R_b &= \sqrt{(d-x)^2 + (h-y)^2} \\ R_c &= \sqrt{(d-x)^2 + (h+y)^2} \\ R_d &= \sqrt{(d+x)^2 + (h+y)^2} \end{aligned} \tag{4}$$

The signal phases T_a, T_b, T_c, and T_d, measured on the four electrodes, are described by Eq. (5).

$$\begin{aligned} T_a &= T_0 + T_{a0} + R_a/c \\ T_b &= T_0 + T_{b0} + R_b/c \\ T_c &= T_0 + T_{c0} + R_c/c \\ T_d &= T_0 + T_{d0} + R_d/c \end{aligned} \tag{5}$$

Here, T_0 is the arrival time of the bunch crossing the detection electrode plane, and T_{a0}, T_{b0}, T_{c0}, and T_{d0} are the transmission delays of the four measurement channels.

By subtracting the arrival time and transmission delays from the original signal phase measurements, we can obtain the transverse distances R_a, R_b, R_c, and R_d between the beam bunch and four electrodes. (The subtraction method is discussed later.) Therefore, the absolute transverse position of the bunch can be determined by drawing circles around the two electrodes, as shown in Fig. 3. The electrodes were used as the centers of the circles, and the propagation distance was used as the radius.

When the transverse distances of the bunch are obtained, only circular paths with radius R_a around Electrode A can contain the beam bunch (blue dotted line in Fig. 3). Similarly, only circular paths with radius R_b around Electrode B can contain a beam bunch (red dotted line in Fig. 3). The intersection point of these two circles can be used to determine the transverse position of the bunch, and this can be achieved by using the signal phase (arrival time).

As previously mentioned, the bunch transverse position and signal phase measurement uncertainty exhibit a linear relationship. Consequently, there is a direct correlation between the phase-measurement uncertainty and transverse-position measurement uncertainty. Assuming that the phase-measurement uncertainty is ΔT, the transverse-position measurement uncertainty is $\Delta R = \Delta T \times c$.

In the commonly used Cartesian coordinate system, determining the transverse position (x, y) of a bunch for various distances between two electrodes involves more complex relationships than those described above. Figure 4 illustrates several typical relationships.

Black stars represent the true positions of the bunches, while blue and red dashed lines indicate the possible area boundaries of the bunch. The circle surrounded by the blue dotted line represents the area where a bunch may appear under the phase measurement uncertainty of Electrode A. The circle surrounded by the red dotted line represents the area where the bunch may appear under the phase measurement uncertainty of Electrode B. Therefore, the transverse bunch can be located anywhere within these overlapping regions (marked by a purple circle). The bunch transverse position measurement uncertainty obtained using this method depends not only on the signal phase measurement uncertainty, but also on the relative geometric

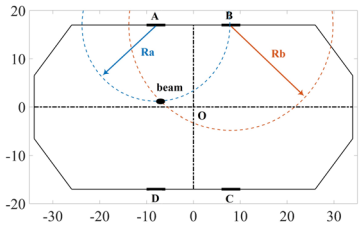

Fig. 3 Determination of the bunch transverse position by finding the intersection point of two circles

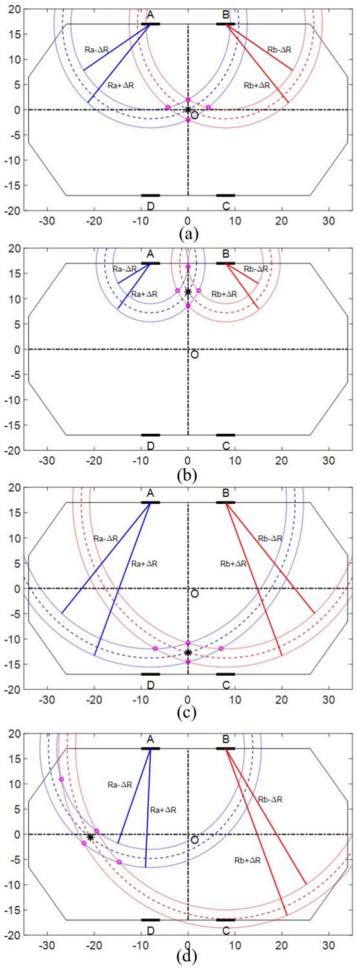

Fig. 4 Transverse position uncertainty introduced by signal phase measurement uncertainty: **a** bunch close to the chamber center, **b** bunch with a large vertical offset near the upper buttons, **c** bunch with a large vertical offset near the lower buttons, and **d** bunch with a large horizontal offset

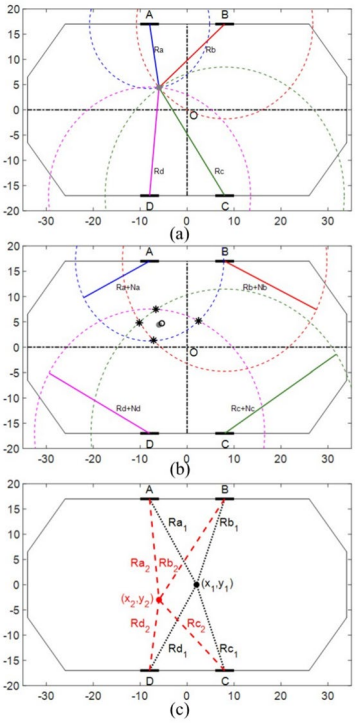

Fig. 5 **a** Pairing of adjacent electrodes to solve the bunch transverse position using the four intersection points in the ideal case. **b** Pairing of adjacent electrodes to solve the bunch transverse position using the four intersection points with measurement error. **c** Same bunch passes through different transverse positions in different turns

relationship between the bunch and detection electrodes. When the beam passed near the center of the vacuum chamber (Fig. 4a), the measurement errors in the horizontal and vertical planes are relatively small and equivalent. When the beam eccentrically passes through the side of the electrode in the vertical plane (Fig. 4b), the measurement error in the horizontal plane is relatively small, whereas that in the vertical plane is relatively large. When the beam passes through the side of the electrode with an eccentricity in the vertical plane (Fig. 4c), the measurement error in the vertical plane is small, whereas that in the horizontal plane is large. When the beam passes eccentrically along the horizontal plane (Fig. 4d), a significant measurement error exists in both the horizontal and vertical planes.

In practice, we obtained four signal phase results from the four electrodes. Ideally, these four sets should overlap completely, as shown in Fig. 5a.

However, owing to systematic and random measurement errors in each channel, these four intersection points no longer completely overlap, as shown in Fig. 5b.

In this case, considering any intersection point as a measurement results in large errors. There are four intersection points, and their mathematical average (marked by black circles) is very close to the true position of the beam bunch (gray dotted line).

The final signal phase includes three contributions, as shown in Eq. (3). Only the third part of the signal was used in the triangulation positioning method to determine the bunch transverse position. The remaining values can be regarded as measurement system constants that need to be calibrated. During the actual data analysis processes, we continuously collected the sampled bunch-phase signals for multiple cycles at a given sampling rate. During the data acquisition, the transmission delay of each channel remained constant. Furthermore, the differences in the arrival times of successive cycles were constant. For example, if we record data with different transverse positions of (x_1, y_1) and (x_2, y_2) across two adjacent cycles as shown in Fig. 5c, we obtain four equations involving four unknowns as shown in Eq. (6).

$$
\begin{aligned}
T_{a1} - T_{a2} &= \Delta T_0 + (R_{a1} - R_{a2}) \Big/ c \\
T_{b1} - T_{b2} &= \Delta T_0 + (R_{b1} - R_{b2}) \Big/ c \\
T_{c1} - T_{c2} &= \Delta T_0 + (R_{c1} - R_{c2}) \Big/ c \\
T_{d1} - T_{d2} &= \Delta T_0 + (R_{d1} - R_{d2}) \Big/ c
\end{aligned} \tag{6}
$$

When we use (x_1, y_1) and (x_2, y_2) to represent R, all variables in the equation, except for x and y, can be obtained. Therefore, the transverse position can also be solved. Substituting the solved lateral position data into Eq. (6), we can obtain the arrival time (T_0) of the bunch and transmission delays T_{a0}, T_{b0}, T_{c0}, and T_{d0}.

In the actual measurement process, thousands of cycles of data can be continuously obtained; therefore, the calibration accuracy of these two system parameters can be improved by averaging multiple results.

3 Numerical Simulation Analysis

In order to assess the sensitivity and measurement error of the proposed new transverse position measurement method, we used numerical simulations to analyze the dependency between the changes in bunch transverse position and the phase changes of electrode-induced bunch signals. The results are shown in Fig. 6.

Two new combinations of the measured beam bunch signal phases are defined in Eq. (7).

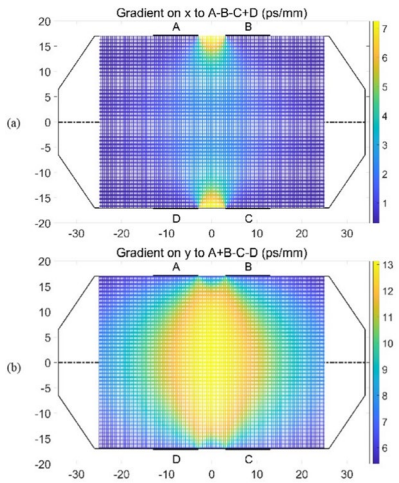

Fig. 6 (Color online) Relationship between the bunch position and phase change combination of the four electrode signals: **a** horizontal gradient and **b** vertical gradient

$$
\begin{aligned}
T_x &= T_a - T_b - T_c + T_d \\
T_y &= T_a + T_b - T_c - T_d
\end{aligned} \tag{7}
$$

We can calculate the change in T_x due to the bunch transverse position change, which represents the horizontal position measurement sensitivity, as shown in Fig. 6a. The sensitivity of the vertical position measurements is shown in Fig. 6b. Similar to the button electrode layout of the SSRF storage ring, there is an approximately linear region near the center of the vacuum chamber with a higher vertical sensitivity (approximately 12 ps mm^{-1}), larger linear region (within a radius of 5 ps mm^{-1}), and lower horizontal sensitivity (approximately 3 ps mm^{-1}). In addition, there is a smaller linear region (within a radius of 2 ps mm^{-1}).

To assess the practicality of the new measurement method, we utilized typical parameters during the injection process of the SSRF top-up mode. We used a residual Betatron oscillation amplitude of 1 mm, horizontal tune of 0.15, and horizontal damping time of 0.3 mm, as shown in Fig. 7. A Monte Carlo simulation was conducted to model the damping decay process of the residual Betatron oscillations in the horizontal direction within 2000 cycles after injection. Simultaneously, the bunch signal phases were measured, and the bunch transverse position was calculated based on the new methods. These results demonstrated the practicality of the proposed method for accurately determining the transverse position of a bunch.

The simulated results show that with a measured error (RMS) of 0.2 ps, the proposed method can accurately measure and record the damping decay process of the transverse position oscillations after injection.

4 Confirmatory Experiments

During the operation of the SSRF, a large amount of bunch-by-bunch data was recorded. This provided favorable conditions for verifying the feasibility of the new measurement principle through bunch experiments. From the operational data collected from 2021 to 2023, four groups of data with different time periods, machine parameters, and significant differences in the bunch behavior were selected to analyze and evaluate the feasibility, accuracy, and measurement errors of the new method.

Comparing the traditional processing methods and SSRF probe configuration, traditional horizontal position measurements using the difference-over-sum (Δ/Σ) algorithm should have much smaller measurement errors than the new method. Therefore, during the evaluation experiments, we used the results of the (Δ/Σ) algorithm as a reference. If the results obtained by the (Δ/Σ) algorithm and proposed methods are consistent, the measurement results of the new

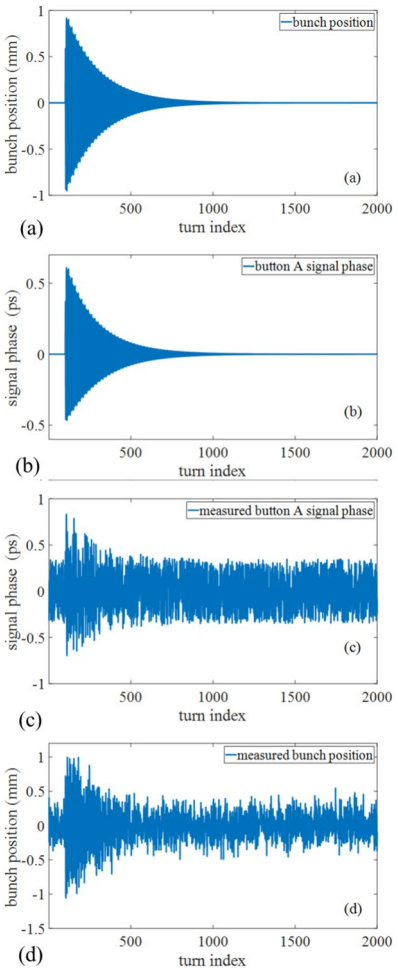

Fig. 7 Monte Carlo simulation results in the horizontal plane after injection: **a** Bunch horizontal position, **b** bunch signal phase detected by Electrode A, **c** measured bunch signal phase with a random noise of 0.2 ps, and **d** measured bunch horizontal position using the four electrode signal phases

method are considered accurate and reliable. Specific data analysis and comparison methods are shown in Fig. 8.

To compare the results of the two methods more efficiently and comprehensively, we employed two different data representations for analysis in both time and frequency domains. In the first representation, we can select any bunch (in this case, bunch #6) and directly compare its multi-turn transverse position waveform in the time domain. In the second representation, we utilized the multi-turn transverse position waveforms of all bunches, calculated their power density spectra, and summarized and presented all information of the bunches in a waterfall plot for comparison in the frequency domain.

The first data sample was obtained during the SSRF machine study cycle to tune the third harmonic cavity. A long train with 500 consecutive bunches was filled with a total beam current of 200 mA. The collected and analyzed data represented the transient injection process, resulting in significant transverse perturbations in the horizontal plane at the moment of injection.

Figure 8a and c shows the transverse position data measured using the conventional (Δ/Σ) method. As shown in the time-domain waveform in Fig. 8a, each bunch exhibits typical approximate damped harmonic oscillations within several tens of turns after the injection moment, consistent with theoretical expectations. In contrast, the power spectral distribution calculated from the transverse position data of all bunches shown in Fig. 8c reveals that the peak frequency and quality factor of the beta oscillation resonance peak exhibit a significant dependence on the intra-bunch index. Each beta oscillation resonance peak was accompanied by a noticeable energy oscillation sideband. Figure 8 b and d presents the transverse position data measured using the new method, which demonstrates complete agreement with the results obtained from the traditional methods, albeit with larger random errors.

The second data sample was obtained during the SSRF user operation cycle. A filling pattern with four short bunch trains (125 bunches per train) at equal intervals was selected; the total beam current was 200 mA. The collected data represent the injection transient process, which results in significant transverse perturbations in the horizontal plane at the moment of injection.

Figure 8e and g shows the transverse position data measured using the traditional (Δ/Σ) method. As shown in the time-domain waveform in Fig. 8e, each bunch exhibited typical approximate damped harmonic oscillations within several tens of turns after the injection moment, similar to the previous data group. The results also indicated a significant intra-bunch position dependence of the beta oscillations, as shown in Fig. 8g. However, no noticeable energy oscillation sideband was observed in this dataset. Figure 8b and h presents the transverse position data measured using the new method, which demonstrates complete agreement with the results obtained from the traditional methods, albeit with larger random errors.

The third data sample was collected during the user operation cycle, with the same bunch-filling pattern and total beam current as the previous dataset. However, the transverse oscillation damping time was much longer.

Compared with the previous two datasets, the time-domain waveform shown in Fig. 8i of this dataset exhibits a significantly longer transverse oscillation damping process, consistent with the theoretical expectations. The power spectral distribution in Fig. 8k shows that apart from some differences in the oscillation amplitude, there is no significant intra-bunch position dependence of the peak frequency or quality factor of the beta oscillation resonance peak. Figure 8j and l presents the transverse position data measured using the new method, which clearly

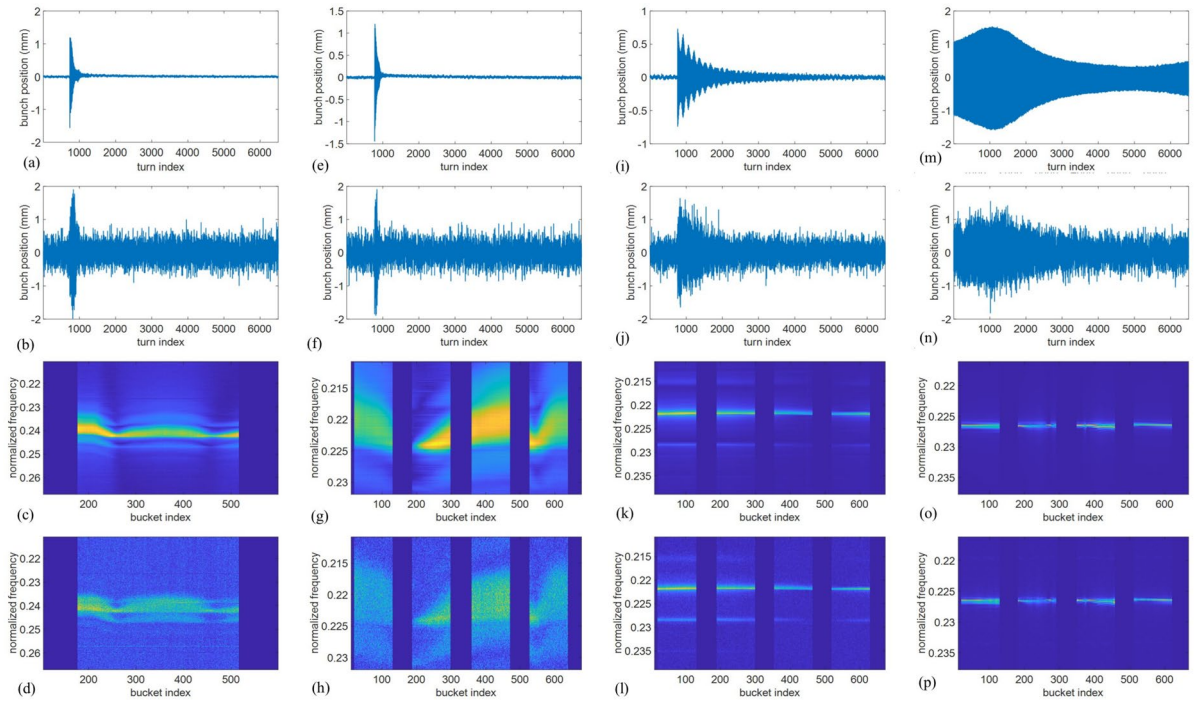

Fig. 8 (Color online) **a**, **b**, **c**, and **d** Analysis results of the injection data acquired on December 20, 2021. **e**, **f**, **g**, and **h** Analysis results of the injection data acquired on January 15, 2022. **i**, **j**, **k**, and **l** Analysis results of the injection data acquired on March 5, 2022. **m**, **n**, **o**, and **p** Analysis results of the injection data acquired on March 21, 2023. **a**, **e**, **i**, and **m** Horizontal position waveform of bunch #6 obtained by the (Δ/Σ) method. **b**, **f**, **j**, and **n** Horizontal position waveform of bunch #6 obtained by the new method. **c**, **g**, **k**, and **o** Frequency spectrogram of all bunch horizontal positions calculated by the (Δ/Σ) method. **d**, **h**, **l**, and **p** Frequency spectrogram of all bunch horizontal positions calculated by the new method

demonstrates complete agreement with the results obtained from traditional methods, albeit with larger random errors.

The last sample was captured during user operation when multi-bunch transverse instabilities occurred. The bunch-filling pattern and total beam current were identical to those of the previous dataset.

Although there were no injection disturbances, strong transverse instabilities in occurred in the multi-bunch during operation. Consequently, each bunch experienced transverse oscillations with varying amplitudes over time, as shown in the typical time-domain waveform in Fig. 8m. The power spectral distributions shown in Fig. 7o reveal that the beta oscillation of each bunch was no longer a single-frequency resonance peak but rather had a fine structure, which was particularly evident for bunch #400. The results obtained using the proposed method are presented in Figs. 8n and p; these results are identical to those obtained from Figs. 8m and o.

In addition to verifying the accuracy of the new measurement method using the aforementioned four typical data samples, we used principal component analysis (PCA) to evaluate and compare the position measurement uncertainties of the two methods [35], as shown in Fig. 9.

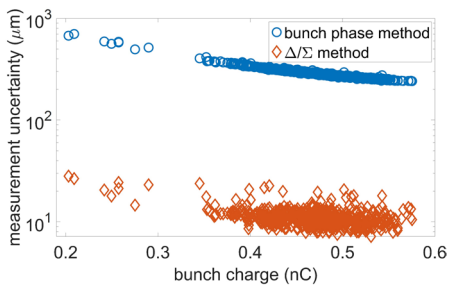

Fig. 9 Measurement uncertainty of the two methods

The conventional method, calculating transverse position using the signal amplitude of four electrodes, can achieve a bunch position resolution as good as 10 microns (marked with a red diamond symbol in Fig. 9). Under the same conditions, the newly proposed measurement method based on the phase difference of electrode signals, before further optimization of the signal phase extraction algorithm, is temporarily unable to achieve the same performance (marked with a blue circle in Fig. 9) was better than 250 μm, consistent with the level of horizontal position sensitivity predicted based on numerical simulations.

5 Discussion

In this study, the viability of a novel approach in determining the absolute transverse position of a bunch was investigated. Numerical simulations and experimental results under various conditions demonstrate that the bunch-by-bunch absolute transverse position can be determined by analyzing the phase differences detected by different electrodes.

However, the current electrode layout and signal-phase detection techniques used in the SSRF storage rings have not been optimized to support high-resolution bunch-by-bunch transverse-position measurements using this new method. Compared with the traditional method based on the (Δ/Σ) algorithm, the random measurement errors were more than an order of magnitude larger. Because the measurement error of the new method solely depends on the accuracy of the phase measurement, there are various ways to improve the system resolution. For example, the electrode structure and layout can be improved, electrodes sensitive to arrival time response can be developed, or electrodes can be oriented toward the center of the closed trajectory. Signal-conditioning circuits and analysis algorithms for phase measurements also require improvement. The current approach involved directly collecting the BPM electrodes and then applying appropriate signal conditioning methods, such as filtering, which can enhance the accuracy of the phase measurement and consequently improve the accuracy of the measurements obtained using the new method. Despite the higher random measurement errors at this stage, the proposed method has unique application values in certain special cases because it yields the absolute position as the measurement result. For instance, it can be used for the in situ calibration of the sensitivity coefficient of a traditional BPM system.

In addition to these advantages, this new measurement method offers several other benefits. The relationship between the changes in the transverse position and those in the measured phase was approximately linear, regardless of the vacuum chamber aperture parameters (distance from the detector electrode to the center of the pipe). By contrast, the conventional (Δ/Σ) method exhibits a linear relationship with respect to this distance. The random measurement errors for the traditional methods increased with increasing vacuum chamber aperture, whereas those for the new method remained constant, probably even outperforming the traditional methods for large vacuum chamber sizes. The mapping between the transverse position and actual signal phase was independent of the bunch or bunch length.

6 Conclusion

This paper presented a novel method for measuring the absolute transverse position of bunches. By utilizing the geometric relationship between the center position of a measured bunch and multiple detection electrodes and analyzing the time difference in the arrival time of the bunch signals detected by these electrodes, the absolute transverse position of the bunch when crossing the detection electrode plane was calculated.

Numerical simulations and experimental results from an SSRF storage ring demonstrated the feasibility and accuracy of this method. Because of the lack of optimization specific to signal phase extraction, the position resolution of this method is lower than that of traditional methods based on signal amplitude extraction. However, this method offers distinctive advantages, such as absolute position measurements, a position sensitivity coefficient that is independent of the vacuum chamber aperture, and detector electrode layout flexibility. With further optimization efforts, the performance of this new method could be improved significantly. Overall, this new method shows promise for specific applications and warrants further development and broader adoption.

Author Contributions All authors contributed to the study conception and design. Material preparation, data collection and analysis were performed by Xing Yang, Hong-Shuang Wang and Yi-Mei Zhou. The first draft of the manuscript was written by Xing Yang, and all authors commented on previous versions of the manuscript. All authors read and approved the final manuscript.

Data Availability The data that support the findings of this study are openly available in Science Data Bank at https://cstr.cn/31253.11.sciencedb.j00186.00184 and https://www.doi.org/10.57760/sciencedb.j00186.00184.

Declarations

Conflict of interest Yong-Bin Leng is an editorial board member for Nuclear Science and Techniques and was not involved in the editorial review, or the decision to publish this article. All authors declare that there are no conflict of interest.

References

1. C. Evain, F. Kaoudoune, E. Roussel et al., Stabilization of the bunch position during the control of the microbunching instability in storage rings. Phys. Rev. Accel. Beams **26**, 090701 (2023). https://doi.org/10.1103/PhysRevAccelBeams.26.090701
2. A. Streun, M. Aiba, M. Böge et al., Swiss Light Source upgrade lattice design. Phys. Rev. Accel. Beams **26**, 091601 (2023). https://doi.org/10.1103/PhysRevAccelBeams.26.091601
3. R. E. Shafer, Beam position monitoring. InL AIP Conference Proceedings 212, Upton, New York, pp. 26–58 (1989). https://doi.org/10.1063/1.39710

4. J. He, Y.F. Sui, Y. Li et al., Design and fabrication of button-style beam position monitors for the HEPS synchrotron light facility. Nucl. Sci. Tech. **33**, 141 (2022). https://doi.org/10.1007/s41365-022-01126-7
5. G. Valentino, G. Baud, R. Bruce et al., Final implementation, commissioning, and performance of embedded collimator beam position monitors in the Large Hadron Collider. Phys. Rev. Accel. Beams **20**, 081002 (2017). https://doi.org/10.1103/PhysRevAccelBeams.20.081002
6. Z.C. Chen, Y.B. Leng, K.R. Ye et al., Beam position monitor design for a third generation light source. Phys. Rev. ST Accel. Beams **17**, 112801 (2014). https://doi.org/10.1103/PhysRevSTAB.17.112801
7. Y. Balkova, M. Urbaniak, A. Makhnev et al., New Beam Position Detectors for NA61/SHINE experiment. J. INST. **17**, 08019 (2022). https://doi.org/10.1088/1748-0221/17/08/C08019
8. Y. Shobuda, Y.H. Chin, Optimization of electrode shape for stripline beam position monitors. Phys. Rev. ST Accel. Beams **17**, 092801 (2014). https://doi.org/10.1103/PhysRevSTAB.17.092801
9. M. Wendt, M. Barros Marin, A. Boccardi et al., Technology and first beam tests of the new CERN-SPS beam position system. In: Paper presented at the 8th International Beam Instrumentation Conference, Malmö, Sweden, 08–12 September 2019. https://doi.org/10.18429/JACoW-IBIC2019-WEPP046
10. X.Y. Liu, F.F. Wu, T.Y. Zhou et al., Design and offline testing of a resonant stripline beam position monitor for the IRFEL project at NSRL. Nucl. Sci. Tech. **31**, 70 (2020). https://doi.org/10.1007/s41365-020-00778-7
11. M. Kumar, A. Ojha, A.D. Garg et al., Analytical expression for position sensitivity of linear response beam position monitor having inter-electrode cross talk. Nucl. Instrum. Meth. A. **844**, 90–95 (2017). https://doi.org/10.1016/j.nima.2016.11.048
12. M. Kumar, L.K. Babbar, R.K. Deo et al., Modified coaxial wire method for measurement of transfer impedance of beam position monitors. Phys. Rev. Accel. Beams **21**, 052801 (2018). https://doi.org/10.1103/PhysRevAccelBeams.21.052801
13. J. Chen, Y.B. Leng, S.S. Cao et al., Optimized design method study for cavity BPM system. Nucl. Instrum. Meth. A. **1044**, 167509 (2022). https://doi.org/10.1016/j.nima.2022.167509
14. S. Zorzetti, M. Wendt, H. Mainaud-Durand, Characterization and alignment of a resonant cavity beam position monitor for the Compact LInear Collider (CLIC) project at CERN. Nucl. Instrum. Meth. A **1048**, 167898 (2023). https://doi.org/10.1016/j.nima.2022.167898
15. J. Chen, Y.B. Leng, L.Y. Yu, Optimization of the cavity beam-position monitor system for the Shanghai Soft X-ray Free-Electron Laser user facility. Nucl. Sci. Tech. **33**, 124 (2022). https://doi.org/10.1007/s41365-022-01117-8
16. H. Maesaka, H. Ego, S. Inoue et al., Sub-micron resolution rf cavity beam position monitor system at the SACLA XFEL facility. Nucl. Instrum. Meth. A. **696**, 66–74 (2012). https://doi.org/10.1016/j.nima.2012.08.088
17. D.R. Bett, N.B. Kraljevic, T. Bromwich et al., High-resolution, low-latency, bunch-by-bunch feedback system for nanobeam stabilization. Phys. Rev. Accel. Beams **25**, 022801 (2022). https://doi.org/10.1103/PhysRevAccelBeams.25.022801
18. T. Shintake, M. Tejima, H. Ishii et al., Sensitivity calculation of beam position monitor using boundary element method. Nucl. Instrum. Meth. A. **254**(1), 146–150 (1987). https://doi.org/10.1016/0168-9002(87)90496-7
19. M. Shafiee, S.A.H. Feghhi, J. Rahighi, Numerical analysis of the beam position monitor pickup for the Iranian light source facility. Nucl. Instrum. Meth. A. **847**, 162–170 (2017). https://doi.org/10.1016/j.nima.2016.11.065
20. J. He, Y.F. Sui, Y. Li et al., Design and optimization of a Goubau line for calibration of BPMs for particle accelerators. Nucl. Instrum. Meth. A. **1045**, 167635 (2023). https://doi.org/10.1016/j.nima.2022.167635
21. N. Zhang, Y.B. Leng, Z.C.Chen et al., A bunch-by-bunch beam position monitor based on scope embedded IOC. Nucl. Tech. (in Chinese) **35**, 337–341 (2012)
22. Y.M. Zhou, H.J. Chen, S.S. Cao, Bunch-by-bunch longitudinal phase monitor at SSRF. Nucl. Sci. Tech. **29**, 113 (2018). https://doi.org/10.1007/s41365-018-0445-6
23. Y.M. Zhou, Y.B. Leng, X.Y. Xu, Signal processing algorithm optimization of bunch-by-bunch phase measurement system for storage ring. High Power Laser Particle Beams (in Chinese) **32**, 074002 (2020). https://doi.org/10.11884/HPLPB202032.200033
24. Y.M. Zhou, X.Y. Xu, Y.B. Leng, Precise measurement and application of synchrotron tune at storage ring. Nucl. Tech. (in Chinese) **44**, 090103 (2021). https://doi.org/10.11889/j.0253-3219.2021.hjs.44.090103
25. B. Gao, L.W. Lai, X.Q. Liu et al., Research and applications of bunch purity monitor at SSRF. Nucl. Tech. (in Chinese) **44**, 030101 (2021). https://doi.org/10.11889/j.0253-3219.2021.hjs.44.030101
26. X.Y. Xu, Y.B. Leng, Y.M. Zhou et al., Bunch-by-bunch three-dimensional position and charge measurement in a storage ring. Phys. Rev. Accel. Beams **24**, 032802 (2021). https://doi.org/10.1103/PhysRevAccelBeams.24.032802
27. X.Y. Xu, Y.B. Leng, B. Gao, HOTCAP: A new software package for high-speed oscilloscope-based three-dimensional bunch charge and position measurement. Nucl. Sci. Tech. **32**, 131 (2021). https://doi.org/10.1007/s41365-021-00966-z
28. Z. Zhang, Y.B. Zhao, K. Xu et al., Low level radio frequency controller for superconducting third harmonic cavity at SSRF. Nucl. Tech. (in Chinese) **45**, 120101 (2022). https://doi.org/10.11889/j.0253-3219.2022.hjs.45.120101
29. K.L. Liao, X. Zheng, Z. Li et al., Development of a grazing incidence X-ray diffractometer for BL02U2 at SSRF. Nucl. Tech. (in Chinese) **46**, 120101 (2023). https://doi.org/10.11889/j.0253-3219.2023.hjs.46.120101
30. S. Krishnamoorthy, J.P. Schmall, S. Surti, In Basic Science of PET Imaging, ed. by M.M. Khalil (Springer, Cham 2016), pp. 173–197. https://doi.org/10.1007/978-3-319-40070-9
31. Q.Y. Wei, T.P. Xu, T.T. Dai et al., Development of a compact DOI-TOF detector module for high-performance PET systems. Nucl. Sci. Tech. **28**, 43 (2017). https://doi.org/10.1007/s41365-017-0202-2
32. J.N. Dong, Y.L. Zhang, Z.Y. Zhang et al., Position-sensitive plastic scintillator detector with WLS-fiber readout. Nucl. Sci. Tech. **29**, 117 (2018). https://doi.org/10.1007/s41365-018-0449-2
33. C.H. Miao, M. Liu, H. Shu et al., Design of a proton spot scanning position control system. Nucl. Tech. (in Chinese) **41**, 040201 (2018). https://doi.org/10.11889/j.0253-3219.2018.hjs.41.040201
34. N. Yu, Y.P. Xu, Y.K. Cai et al., Simulation study on time resolution optimization of silicon drift detector. Nucl. Tech. (in Chinese) **44**, 040404 (2021). https://doi.org/10.11889/j.0253-3219.2021.hjs.44.040404
35. H.J. Chen, J. Chen, B. Gao et al., Bunch-by-bunch beam size measurement during injection at Shanghai Synchrotron Radiation Facility. Nucl. sci. Tech. **29**, 79 (2018). https://doi.org/10.1007/s41365-018-0420-2